Mon. Not. R. Astron. Soc. **000**, 1–?? (3004) Printed 4 February 2013 (MN LATEX style file v2.2)

Non-equilibrium cooling rate for a collisionally cooled metal-enriched gas

Evgenii O. Vasiliev[1⋆]
[1] *Institute of Physics, Department of Physics, Southern Federal University, Stachki Ave. 194, Rostov-on-Don, 344090 Russia*

Accepted 3004 December 15. Received 2004 December 14; in original form 2004 December 31

ABSTRACT

We present self-consistent calculations of non-equilibrium (time-dependent) cooling rates for a dust-free collisionally controlled gas in wide temperature ($10\ K \leqslant T \leqslant 10^8\ K$) and metallicity ($10^{-4}\ Z_\odot \leqslant Z \leqslant 2\ Z_\odot$) ranges. We confirm that molecular hydrogen dominates cooling at $10^2 \lesssim T \lesssim 10^4$ K and $Z \lesssim 10^{-3}\ Z_\odot$. We find that the contribution from H_2 into cooling rate around $T \sim (4-5)\times10^3$ K stimulates thermal instability in the metallicity range $Z \lesssim 10^{-2}\ Z_\odot$. Isobaric cooling rates are generally lower than isochoric ones, because the associated increase of gas density leads to both more efficient hydrogen recombination and equilibration of the fine-structure level populations. Isochoric cooling keeps the ionization fraction remains quite high at $T \lesssim 10^4$ K: up to ~ 0.01 at $T \simeq 10^3$ K and $Z \lesssim 0.1\ Z_\odot$, and even higher at higher metallicity, contrary to isobaric cooling where it at least an order of magnitude lower. Despite this increase in ionization fraction the gas-phase formation rate of molecular hydrogen (via H^-) lowers with metallicity, because higher metallicity shorttens the evolution time. We implement our self-consistent cooling rates into the multi-dimensional parallel code ZEUS-MP in order to simulate evolution of a supernova remnant, and compare it with an analogous model with tabulated cooling rates published in previous works. We find significant differences between the two descriptions, which may appear, e.g., in mixing of the ejected metals in the circumstellar medium.

Key words: atomic processes - molecular processes – plasmas - galaxies: general – intergalactic medium - ISM

1 INTRODUCTION

A choice between equilibrium and non-equilibrium (time-dependent) cooling rates in collisionally controlled gas strongly depends on the ratio between dynamical and chemical/cooling times. Calculations of the cooling rates of astrophysical plasma in the collisional ionization equilibrium (CIE) for $T \gtrsim 10^4$ K were performed by many authors (House 1964; Cox & Tucker 1969; Raymond et al. 1976; Shull & van Steenberg 1982; Gaetz & Salpeter 1983; Böhringer & Hensler 1989; Sutherland & Dopita 1993; Landi & Landini 1999; Benjamin et al. 2001; Bryans et al. 2006; Schure et al. 2009). However, calculations of the time-dependent ionization of metals and associated radiative cooling rates showed significant deviations from the CIE states and rates (Kafatos 1973; Shapiro & Moore 1976; Edgar & Chevalier 1986; Schmutzler & Tscharnuter 1993; Sutherland & Dopita 1993; Gnat & Sternberg 2007; de Avillez & Breitschwerdt 2010; Vasiliev 2011).

A more complex task is a calculation of cooling rate below 10^4 K, because we need to take into account many processes between atomic and molecular species (e.g., Dalgarno & McCray 1972; Hollenbach & McKee 1979, 1989). Apart from these difficulties a level of the calculation complexity of the cooling rate depends on one's purposes and typical timescales of physical problem considered. Under some conditions chemical network at $T < 10^4$ K can be constrained significantly. For example, Abel et al. (1997) and Galli & Palla (1998) proposed the reduced chemical network for the primordial gas, Glover & Jappsen (2007) considered the chemistry of the metal-enriched interstellar medium. Sometimes, only cooling rates (without solving chemical kinetics equations) are used to study the interstellar medium, for instance, the rates calculated by Dalgarno & McCray (1972) are applied widely.

Usually the cooling rates are provided separately in two temperature ranges, the first is $T = 10^4 - 10^8$ K (e.g., Raymond et al. 1976; Sutherland & Dopita 1993; Bryans et al. 2006; Gnat & Sternberg 2007) and the second is $T \lesssim 10^4$ K (e.g., Dalgarno & McCray 1972;

⋆ E-mail:eugstar@mail.ru

Hollenbach & McKee 1989). Very rarely the rates are presented in both ranges (e.g., Spaans & Norman 1997). This is explained by difference in physical problems considered by authors. But very frequently one needs cooling rates in both ranges. So that usually high- and low-temperature cooling rates are combined from different tables, where the rates were computed using different assumptions. Thus, it is necessary to conduct a self-consistent calculation of cooling rate within both high- and low-temperature ranges.

In this paper we present self-consistent calculations of non-equilibrium cooling rates of a collisionally cooled metal-enriched dust-free gas in wide temperature range, $10\ K \leqslant T \leqslant 10^8\ K$, and we study dependence of the rates on metallicity and density. A possible influence from dust grains and external ionizing radiation field will be considered elsewhere. The paper is organized as follows. In Section 2 we briefly describe the details of the model. In Sections 3 and 4 we present our results. In Section 5 we study the supernova shell evolution using newly calculated cooling rates. In Section 6 we summarize our results.

2 MODEL DESCRIPTION

The chemical and thermal evolution of a gas parcel can be divided into a high-temperature ($T > 2 \times 10^4$ K) and a low-temperature ($T \leqslant 2 \times 10^4$ K) ranges. Such division can be explained by the transition to neutral gas and the formation of molecules in the latter range. The full description of the method and the references to the atomic data for the former temperature range can be found in Vasiliev (2011). Briefly, in our calculations we consider all ionization states of the elements H, He, C, N, O, Ne, Mg, Si and Fe. We take into account the following major processes in a collisional gas: collisional ionization, radiative and dielectronic recombination as well as charge transfer in collisions with hydrogen and helium atoms and ions.

To study the chemical evolution of a low-temperature ($T \leqslant 2 \times 10^4$ K) gas we should take into account molecules, especially molecular hydrogen, which is expected to be the most significant coolant in a gas with metallicity below $10^{-3} Z_\odot$. Hence, the above-listed ionization states of the elements is replenished by a standard set of species: H^-, H_2, H_2^+, D, D^+, D^-, HD, needed to model the H_2/HD gas-phase kinetics (Abel et al. 1997; Galli & Palla 1998). The corresponding rates are taken from Galli & Palla (1998); Stancil et al. (1998); Mac Low & Shull (1986). The list of the chemical reactions for molecular hydrogen and deuterium chemistry is presented in Appendix 1.

The system of time-dependent ionization state equations should be complemented by the energy equation, which can be written in the form

$$\frac{du}{dt} = \frac{p}{\rho^2}\frac{d\rho}{dt} - L \tag{1}$$

where $u = p/(\gamma - 1)\rho$ is the thermal energy, p is the gas pressure, ρ is the gas density, γ is the adiabatic index, and L is the generalized energy loss function. The equation (1) can be expressed as

$$\frac{1}{\gamma - 1}\frac{dp}{dt} - \frac{\gamma}{\gamma - 1}\frac{p}{\rho}\frac{d\rho}{dt} = -L\rho \tag{2}$$

Table 1. Solar elemental abundances

Element	$(X/H)_\odot$
Helium	0.081
Carbon	2.45×10^{-4}
Nitrogen	6.03×10^{-5}
Oxygen	4.57×10^{-4}
Neon	1.95×10^{-4}
Magnesium	3.39×10^{-5}
Silicon	3.24×10^{-5}
Iron	2.82×10^{-5}

Assuming $\gamma = 5/3$ we find that the gas temperature evolves as (e.g., Kafatos 1973)

$$\frac{dT}{dt} = -\frac{n_e n_H \Lambda}{A n k_B} - \frac{T}{n}\frac{dn}{dt} \tag{3}$$

where n is the total particle density of the gas, n_e and n_H are the electron and total hydrogen number densities, $\Lambda(x_i, T, Z)$ is cooling rate, k_B is the Boltzman constant, A is a constant equal to 3/2 for isochoric and 5/2 for isobaric cooling. The second term in equation (3) reflects the relative change in the number of particles in the unit of volume, such change is very important in gas below $T \lesssim 10^4$ K, where gas recombines rapidly.

The total (except molecular deposit) cooling rate is calculated using the photoionization code CLOUDY (ver. 08.00, Ferland et al. 1998). The radiative losses by H_2 is taken from (Galli & Palla 1998) and the HD cooling rate is taken from (Flower 2000; Lipovka et al. 2005). For the solar metallicity we adopt the abundances reported by Asplund et al. (2005), except Ne for which the enhanced abundance is adopted (Drake & Testa 2005), the solar abundances are listed in Table 1. In our calculations we assume the helium mass fraction $Y_{\rm He} = 0.24$, which corresponds to [He/H]=0.081. Such value is close to observed one (Izotov & Thuan 1998). In general, it would be difficult at this time to exclude any value of $Y_{\rm He}$ inside the range $0.232 - 0.258$ (e.g. Olive 2010). We solve a set of 103 coupled equations (102 for ions, atoms and molecules, and one for temperature) using a Variable-coefficient Ordinary Differential Equation solver[1] (Brown et al. 1989).

In our calculations we don't include the chemical kinetics of carbon monoxide and lithium hydrid, dust and photoionization effects. It is well known that CO and H_2O molecules significantly affect on the thermal state of the interstellar gas (e.g., Hollenbach & McKee 1979; Omukai et al. 2005; Glover & Jappsen 2007). The CO and H_2O cooling rates dominate over the C and O fine-structure cooling in gas with $T \gtrsim 500$ K (e.g., Glover & Jappsen 2007), but whether it is possible to produce enough CO and H_2O molecules in the gas during its cooling timescale. In the next section we show that the CO/H_2O formation timescale is greater than the cooling time, so that such molecules cannot form in significant amounts within timescale considered here. Hence, we can neglect CO/H_2O kinetics in this model. The LiH molecule is a significant coolant only at $T \lesssim 50$ K.

[1] The numerical code is available from http://www.netlib.org/ode/vode.f

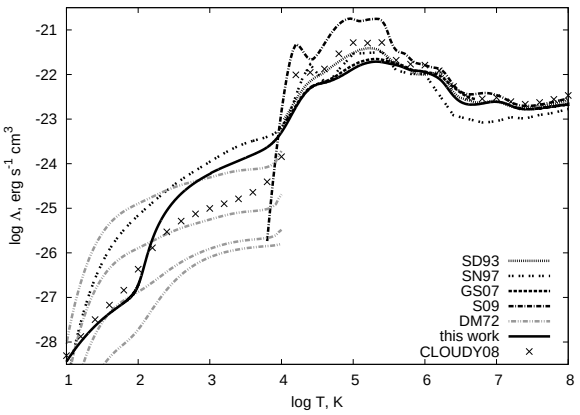

Figure 1. The cooling rates for solar metallicity. The isochoric rate for gas with $n = 1$ cm^{-3} calculated in this work is depicted by solid line. The other lines correspond to the rates obtained in the previous calculations (see text for details).

More important influence on the thermal and chemical evolution is expected from dust and ionizing radiation. Dust particles confine a significant part of metals, produce additional cooling or heating, catalyze the H_2 formation as well. The ionizing radiation ionizes gas and dust. We are going to consider these effects elsewhere. But we note that a simple estimate gives that the H_2 formation on dust grains is inefficient within timescale considered here (see the next section). Several effects from the ionizing radiation on gas at $T > 10^4$ K were described in (Vasiliev 2011).

3 ISOCHORIC COOLING RATES

For isochoric case we start our calculations from $T = 10^8$ K and follow it until the temperature becomes low as $T = 10$ K. In general, the evolution of gas depends on initial ionic composition, temperature and density (see e.g. Sutherland & Dopita 1993; Vasiliev 2012), but here we will consider cooling of gas from very high temperature, so that there is no dependence on initial ionic composition of gas (e.g. Vasiliev 2011, see the next section also). Initially the ionization composition corresponds to the CIE at $T = 10^8$ K obtained from CLOUDY. Figure 1 presents the isochoric cooling rates for a gas with number density $n = 1$ cm^{-3} and solar metallicity. The isochoric rate calculated in this work is depicted by solid line. To compare our calculations of the rates to the previous ones we show the cooling rates obtained by Sutherland & Dopita (1993) (SD93, we have choosen their non-equilibrium data), Spaans & Norman (1997) (SN97), Gnat & Sternberg (2007) (GS07), Schure et al. (2009) (S09), and Dalgarno & McCray (1972) for ionization fraction, $f_i = n_e/n_H = 10^{-4}$, 10^{-3}, 10^{-2}, 0.1, which are shown by dash-dot-dotted lines from bottom to top. The data obtained from CLOUDY code is depicted by crosses (the H_2 molecules are ignored in the equilibrium calculation). One should note that the cooling rates obtained by Sutherland & Dopita (1993), Spaans & Norman (1997), Gnat & Sternberg (2007) were got in non-equilibrium calculations, so that these rates are more or less close to our rate within temperature range $10^4 - 10^6$ K. Spaans & Norman (1997) didn't include high ionization states of metals in their model, so their cooling rate demonstrates significant difference at $T \gtrsim 10^6$ K. The deviation at T below 10^4 K can be explained by different atomic data used in the calculations, and, as a consequence, difference of the ionization states of metals. The cooling curves obtained by Schure et al. (2009) and by using the CLOUDY code are examples of CIE rates, so that significant difference of these rates from non-equilibrium calculations is not a surprise. The Dalgarno & McCray (1972) cooling curves were obtained by simply summing up cooling rates of hydrogen

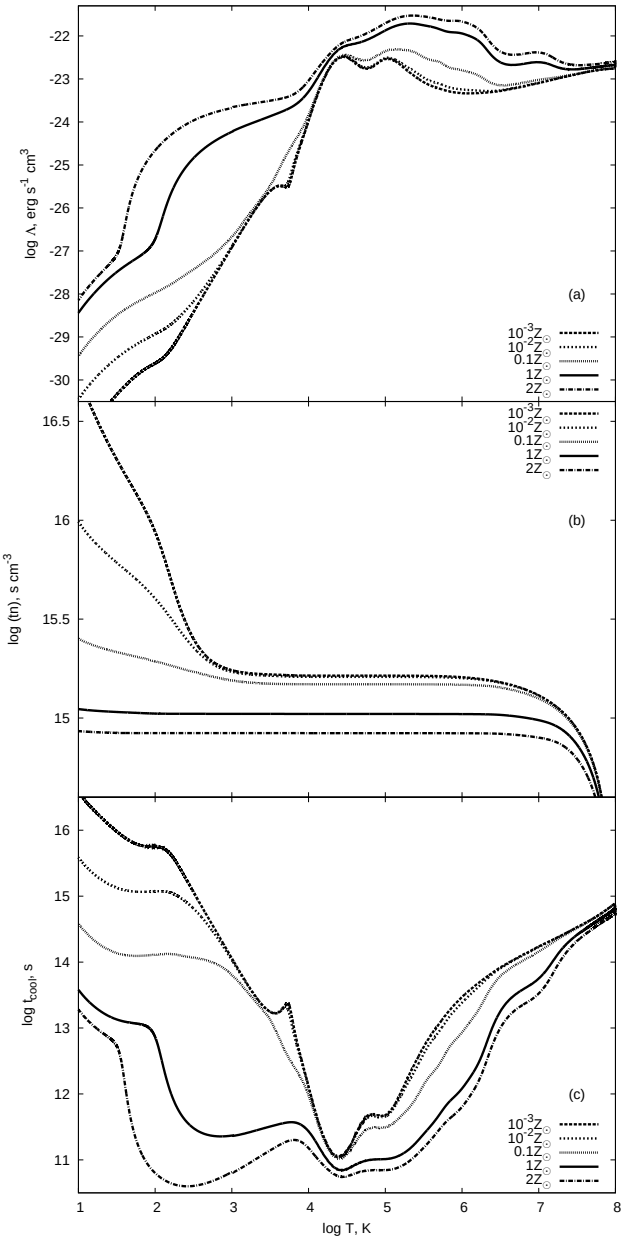

Figure 2. *Upper panel.* The isochoric cooling rates for gas with 10^{-4} $Z_\odot$, 10^{-3} $Z_\odot$, 10^{-2} $Z_\odot$, 0.1 $Z_\odot$, 1 $Z_\odot$, 2 $Z_\odot$ metallicities. The gas density is $n = 1$ cm^{-3}. *Middle panel.* The temperature dependence on the value of fluence, $\eta = \int n dt$ (for isochoric process it is simply $\eta = tn$), for the same gas parameters. *Lower panel.* The isochoric cooling time.

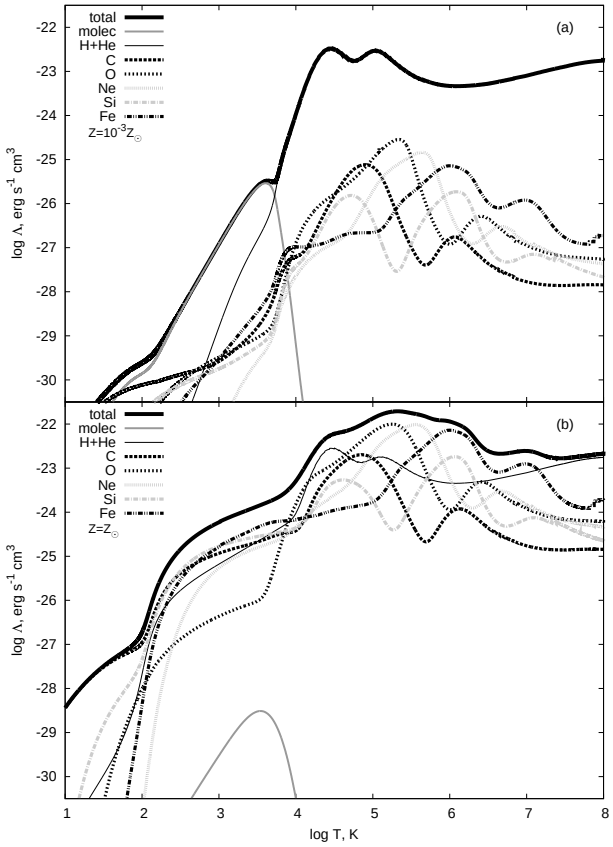

Figure 3. The contributions to the total isochoric cooling rate from each chemical element for 10^{-3} $Z_\odot$ (upper panel) and $Z_\odot$ (lower panel). The contribution by molecules (H_2 and HD) is depicted by grey solid line, the total rate is presented by the thickest solid line, the deposit from H and He is shown by thin solid line.

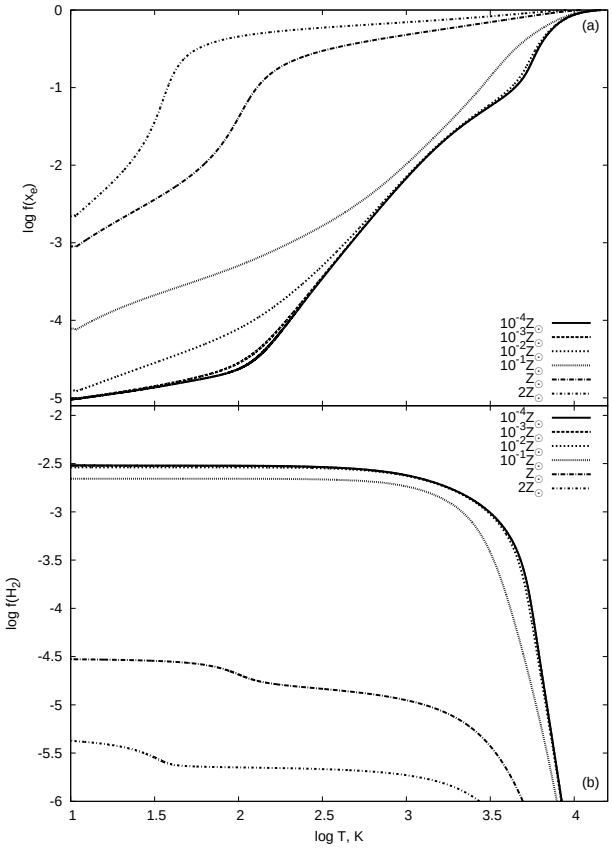

Figure 4. The electron, x_e, (upper panel) and molecular hydrogen, $x_{\rm H_2}$, (lower panel) fractions for metallicities 10^{-4} $Z_\odot$, 10^{-3} $Z_\odot$, 10^{-2} $Z_\odot$, 0.1 $Z_\odot$, 1 $Z_\odot$ and 2 $Z_\odot$ in isochorically cooled gas.

and metals, in which the fractional ionization is used as a free parameter. One can note that our cooling rate is close to the Dalgarno & McCray (1972) rate for $x_e = 0.1$ at $T \sim 10^3 - 10^4$ K and drops to that for $x_e = 10^{-4}$ at $T \lesssim 10^2$ K. This proves a necessity of self-consistent calculations of cooling rates.

Figure 2(upper panel) presents non-equilibrium cooling rates for a dust-free collisionally controlled gas in wide temperature ($10\ K \leqslant T \leqslant 10^8\ K$) and metallicity ($10^{-4}\ Z_\odot \leqslant Z \leqslant 2\ Z_\odot$) ranges. The middle panel shows the temperature evolution (we present the dependence on fluence, $\eta = \int n dt$, which is for isochoric process $\eta = tn$, where t is time elapsed from the beginning of the evolution, n is the number density of gas). Here we should note that all collisional processes are proportional to the square of density. To see clearly the importance of non-equilibrium effects the cooling time, $t_{cool} = k_b T/\Lambda(T)n$, is depicted at lower panel. One can see that the cooling time is comparable with the time elapsed since the beginning of the evolution at very high temperature, $\log T \gtrsim 7.5$, (early time of the evolution) for any metallicity and at low temperature, $\log T \lesssim 2.5$ for $Z \lesssim 10^{-3} Z_\odot$. In other temperature and metallicity ranges the cooling time is shorter than the evolution time, thus, the non-equilibrium effects are significant.

Figure 3 shows the contributions to the total cooling rate from each chemical element and molecules for 10^{-3} $Z_\odot$ (upper panel) and $1 Z_\odot$ (lower panel). Coolants at temperature higher than 10^4 K are described by e.g. Sutherland & Dopita (1993); Schure et al. (2009); Vasiliev (2011). Also it is well-known that below 10^4 K carbon, oxygen and H_2 molecules dominate in cooling depending on metallicity of gas (see, e.g. Hollenbach & McKee 1979, 1989). At very low metallicities, $Z \lesssim 10^{-3}$ $Z_\odot$, molecular hydrogen is the main coolant below 10^4 K. For $Z \sim 10^{-3}$ $Z_\odot$ the contribution from carbon becomes significant only at $T \lesssim 100$ K (upper panel). The increase of metallicity leads to rise of contribution from metals and shortening of temperature range, where the H_2 dominates in cooling. For $Z \gtrsim 0.1$ $Z_\odot$ the H_2 deposit becomes minor at $T < 10^4$ K, e.g. for solar metallicity the molecules produce a negligible cooling rate, whereas the contribution from metals is dominant (lower panel).

One should note that thermal instability can develop at $T \lesssim 10^4$ K. For $Z \lesssim 10^{-2}$ $Z_\odot$ the instability criterion for a gas cooled isochorically (Shchekinov 1978; Chevalier & Imamura 1982)

$$f = \frac{\mathrm{d}\ \ln \Lambda}{\mathrm{d}\ \ln \mathrm{T}} < 1 \qquad (4)$$

is fulfilled around a small bump in the cooling rate at $T \sim (4-5) \times 10^3$ K, which is produced due to the contribution from molecular hydrogen (Figure 3a). The instability

criterion is not reached within $10^{-2} Z_\odot \lesssim Z \lesssim Z_\odot$. Again the conditions favoured to thermal instability can be found for $Z \gtrsim Z_\odot$ at $T \sim (0.8 - 7) \times 10^3$ K (Figure 3b), where the instability develops due to cooling by metals.

The higher metallicity of a gas is the faster evolution goes, or in other words, the cooling time is decreased with the increase of metallicity, e.g. at $T \sim (1 - 10) \times 10^3$ K the cooling timescale for gas with solar metallicity becomes shorter more than ten times compared to that scale for gas with $Z = 0.1\ Z_\odot$ (lower panel of Figure 2). Protons and electrons cannot recombine rapidly and such gas remains overionized: the electron fraction is high as 0.03 at 100K for solar metallicity (Figure 4a). Such fast evolution reveals in decrease of the H_2 fraction (although the H^- fraction is high enough and depends on metallicity weakly: it decreases from $\sim 1.4 \times 10^{-7}$ for $10^{-4}\ Z_\odot$ to 5×10^{-8} for $Z_\odot$, the H_2^+ fraction has the same order), so that for solar metallicity the H_2 fraction decreases more than 100 times compared to its 'universal' value, $(2 - 3) \times 10^{-3}$, (Oh & Haiman 2002), which is reached for $Z \lesssim 0.1\ Z_\odot$ (Figure 4b).

Here we consider the evolution starting from very high temperature, which initially corresponds to the conditions behind strong shock wave, $v \gtrsim 100$ km s^{-1}. Usually it is assumed that dust grains existed in a gas before such shock wave are destroyed behind it, because the destruction time due to thermal sputtering. $\tau \simeq 2 \times 10^4$ yr $(a/0.01\mu\mathrm{m})/n$ (where a is the size of the dust particle, see Draine & Salpeter 1979), is shorter than the cooling time for a gas cooled from $T \gtrsim 10^6$ K depicted in Figure 2c. Moreover, the accretion growth rate is negligible compared to sputtering rate (see Figure 7 in Draine & Salpeter 1979), so that dust grains have no time to reform before the final time is reached in our calculations. Hence, in the present calculations we can do not take into account the H_2 formation on dust grains.

But if dust grains nevertheless exist in a gas, then it is well-established that they catalyze the H_2 production in the interstellar medium (Hollenbach & McKee 1979). In the warm neutral gas ($T \gtrsim 10^3$ K) the H_2 formation of grains dominates over that due to the gas-phase reactions at $Z \gtrsim 0.1\ Z_\odot$ (see the analysis in Glover 2003). The time of H_2 formation on grain-surface is $t^{\mathrm{H_2}}_{grains} \sim 3 \times 10^{16} (T/100)^{-1/2} (nZ/Z_\odot)^{-1}$s (Hollenbach & McKee 1979)[2]. The H_2 formation process can be effective, if the formation time is shorter than the time elapsed from the beginning of the evolution presented in Figure 2b. More exactly, we are interested in the part of the evolution starting from the moment, when the temperature reaches $T \simeq 10^4$ K, to the end the calculation, when $T = 10$ K. Just in this temperature range hydrogen recombines efficiently and H_2 molecules can form on grain surface. This timescale is the same order of magnitude as the full time of the calculation (Figure 2b). One can see that the $t^{\mathrm{H_2}}_{grains}$ is about 1-2 orders of magnitude longer than the time needed to cool from $T \sim 10^4$ K to 10 K. So that, we note that neither grain-surface nor gas-phase H_2 formation channel is effective in a gas with $Z > 0.1\ Z_\odot$, and the H_2 fraction remains negligible (see lower panel of Figure 4).

In general, if dust grains survive after strong shock waves, they contain a significant part of metals. In this case the evolution time of a gas becomes longer and, as a consequence, grain-surface molecule formation becomes more efficient. Because of several additional free parameters, e.g. dust destruction efficiency, depletion factor, we will study the effects from dust on thermal evolution elsewhere.

Another molecules, which can significantly affect the thermal evolution of gas, are CO and H_2O (e.g., Hollenbach & McKee 1979; Glover & Jappsen 2007). These molecules mainly form via reaction channels initiated by the hydroxyl OH (e.g., Hollenbach & McKee 1979). The OH radical forms through reaction between neutral oxygen and molecular hydrogen. Then, the lack of H_2 molecules produces smaller OH fraction. Moreover, as it is mentioned above the H_2 formation on dust grains is inefficient in the conditions considered here, and its fraction decreases with metallicity. The CO formation timescale (for H_2O molecule the timescale is close) is $t(\mathrm{O} \rightarrow \mathrm{CO}) \simeq (10^{-3}/x_{\mathrm{H_2}})(100\mathrm{cm}^{-3}/n)(Z_\odot/Z)$ Myr (Glover & Jappsen 2007). Comparing $t(\mathrm{O} \rightarrow \mathrm{CO})$ with the cooling time, which is $t_{cool} \sim 0.01$ Myr $(1\mathrm{cm}^{-3}/n)$ at $T \sim 10^3 - 10^4$ K for solar metallicity (Figure 2c), it is easy to see that the CO and H_2O molecules will not form in quantities large enough to dominate the cooling.

The higher gas density is the smaller recombination timescales of hydrogen and metals become, so the above-described picture is expected to change in isobaric process.

4 ISOBARIC COOLING RATES

First of all we should choose initial temperature and density of a gas for isobaric calculations. Certainly, to compare with the isochoric models we should start our calculations from $T = 10^8$ K. However we extend our calculations to $T < 10^4$ K, in this range main radiative losses are through fine-structure lines of metals. The level populations of these lines go from equilibrium to non-equilibrium within $n \sim 1 - 100$ cm^{-3} at $T \lesssim 10^3$ K. To catch this transition we should set initial density $n \lesssim 10^{-5}$ cm^{-3} for isobaric calculations started from $T = 10^8$ K. Such density, which is relevant for the intergalactic medium, is quite low for the interstellar medium and, moreover, the cooling time of such gas is larger than the current age of the Universe. For higher density isobaric cooling rates calculated from $T = 10^8$ K have negligible dependence on number density. Hence, to study the transition of level populations of metal fine-structure lines from non-equilibrium to equlibrium we need to take lower initial temperature. But this temperature should be high enough, that initial difference between isochoric and isobaric cooling rates is small and dependence of the evolution on initial temperature is negligible. Using these conditions we can constrain the gas temperature from several$\times 10^5$ to 10^6 K (Gnat & Sternberg 2007; Vasiliev 2012). In this case the compression factor (the ratio of initial temperature to 10^3 K) is about $\lesssim 10^3$ and we can consider number densities $n \gtrsim 10^{-3}$ cm^{-3} as initial values.

[2] A recent analysis of H_2 formation on grain surfaces by Cazaux & Tielens (2004) that takes both physisorbed and chemisorbed hydrogen into account demonstrates that in the conditions of interest in this paper the computed H_2 formation rate is very similar to the widely used rate of Hollenbach & McKee (1979)

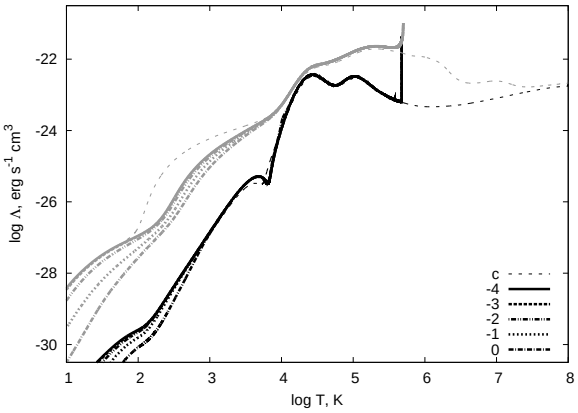

Figure 5. The isobaric (thick lines, numeric labels) and isochoric (thin lines, lablel 'c') cooling rates for metallicities 10^{-3} $Z_\odot$ (black lines), 1 $Z_\odot$ (grey lines). The numeric labels are the logarithm of the initial number density. The initial temperature for the isobaric calculations equals 5×10^5 K. The density of isochorically cooled gas is 0.1 cm^{-3}.

Also we should mention that we consider isobaric compression, which is natural for a gas parcel crossed through strong shock front. So the gas temperature ahead a shock is much lower than the value $T = 3m_p v^2/16k$, where v is a shock front velocity. To mimic this we assume that the ionic composition in a gas before a shock corresponds to that at $T = 2\times10^4$ K. Since here we consider pure collisional ionization model, we should constrain shock wave velocity by a value that does not lead to the radiative precursor formation. A stable photoionization precursor will be formed for shock velocity higher than $v_* \gtrsim 175$ km s^{-1} (Dopita & Sutherland 1996) or shock temperature $T_* = 3m_p v_*^2/16k \gtrsim 7\times10^5$ K. We have found that the cooling rate of a gas behind a shock wave with $T_s \simeq 5\times10^5$ K tends rapidly to the rate in a gas collisionally cooled from $T = 10^8$ K (Vasiliev 2012). Thus, taking into account the above-mentioned constrains on gas temperature we can choose $T = 5\times10^5$ K as initial temperature.

In general, the transition from isobaric to isochoric cooling is controlled by dynamical time of a system: cooling is isobaric when the cooling time is much greater then the dynamical time of a system, $t_c/t_d \gg 1$ and it is isochoric when the time ratio is opposite, $t_c/t_d \ll 1$. For a example, the evolution of a density fluctuation (e.g., a cloud) is determined by the transition from isobaric to isochoric cooling (e.g., Gnat & Sternberg 2007). Such transition is able to determine the characteristic size and mass of the cold dense clumps in two-phase medium (Burkert & Lin 2000).

Figure 5 presents the isobaric cooling rates for gas with metallicity 10^{-3} $Z_\odot$ and 1 $Z_\odot$ (thick lines) and the initial number densities $n = 10^{-4}, 10^{-3}, 10^{-2}, 0.1$ and 1 cm^{-3} (the numeric labels in the Figure are the logarithm of the initial density). As it is mentioned above the initial temperature for the isobaric calculations equals 5×10^5 K. First of all, the tails at $T \sim 5\times10^5$ K are connected with the relaxation of gas behind a shock front (Vasiliev 2012). During this relaxation gas is rapidly ionized, the ionic composition corresponded initially to $T = 2\times10^4$ K tends rapidly to that at $T \sim 5\times10^5$ K. The duration of the period corresponded to

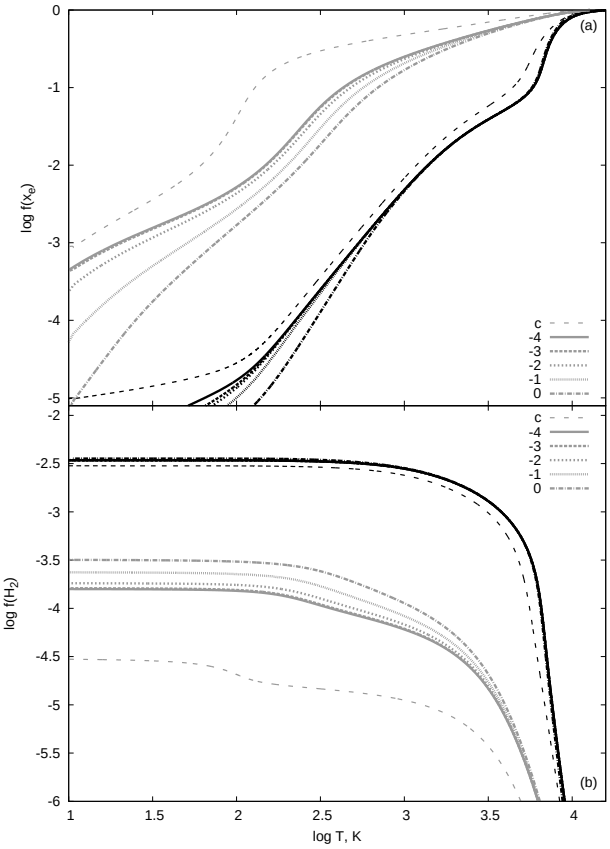

Figure 6. The electron x_e (upper panel) and molecular hydrogen $x_{\rm H_2}$ (lower panel) fractions for metallicities 10^{-3} $Z_\odot$ (black lines), 1 $Z_\odot$ (grey lines) in isobarically cooling gas. The numeric labels are the logarithm of the initial number density. The initial temperature equals 5×10^5 K. The label 'c' corresponds to the isochorically cooled gas with $n = 0.1$ cm^{-3}.

almost constant temperature is very short $\sim 0.01t_f$, where t_f is the total evolution time, which is elapsed from the beginning to that at which the temperature reaches 10 K. But more or less full relaxation reaches during $t \sim 0.1t_f$.

In Figure 5 one can see that the difference between isochoric and isobaric cooling rates reveals at $T \lesssim 10^4$ K. Such difference can be explained by two reasons. At first, the recombination of hydrogen and metals becomes more efficient in a gas with higher density. At second, the cooling below 10^4 K is mainly due to molecule roto-vibrational and metal fine-structure transitions, whose level populations go from non-equilibrium ($L \sim n^2$) to the equilibrium ($L \sim n$) in gas with $n \sim 1 - 10^4$ cm^{-3}. The first (the hydrogen recombination) is significant at $T \sim 10^3 - 10^4$ K, the second (the equilibration) plays a role at $T \lesssim 400$ K.

One can see that for isobarically evolved gas the thermal instability can develop at $T \lesssim 10^4$ K. The instability criterion is weaker than that for isochorically cooling gas (Shchekinov 1978; Chevalier & Imamura 1982)

$$f = \frac{\mathrm{d}\ \ln\ \Lambda}{\mathrm{d}\ \ln\ \mathrm{T}} < 2. \qquad (5)$$

For $Z \lesssim 10^{-2}$ $Z_\odot$ this criterion is fulfilled around a small bump in the cooling rate at $T \sim (4-5)\times10^3$ K, which is produced due to the contribution from molecular hydrogen.

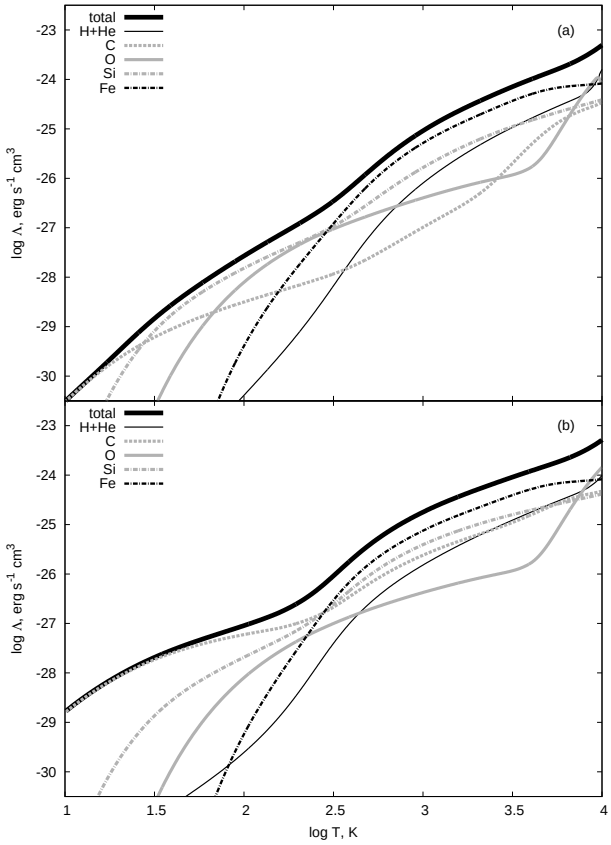

Figure 7. The contributions to the total isobaric cooling rate from major chemical elements for initial number density 1 cm^{-3} (upper panel) and 10^{-2} cm^{-3} (lower panel) for a gas with $Z = Z_\odot$. The initial temperature equals 5×10^5 K.

For gas with $Z \gtrsim Z_\odot$ and initial density $n = 10^{-4}$ cm^{-3} at $T = 5 \times 10^5$ K the temperature range, where the thermal instability can develop, is $T \sim (0.2-10) \times 10^3$ K. This range becomes narrower with increase of initial density, which is explained by steeping of cooling curve (Figure 3b) due to both more efficient hydrogen recombination and equilibration of the fine-structure level populations.

Figure 6 shows the electron (upper panel) and molecular hydrogen (lower panel) fractions for metallicities 10^{-3} $Z_\odot$ (black lines), 1 $Z_\odot$ (grey lines) in gas cooled isobarically. The numeric labels are the logarithm of the initial density. The increase of density intensifies both hydrogen recombination and H_2 molecule formation. For solar metallicity gas the decrease of ionization fraction compared to that for gas cooled isochorically is significant and reaches 0.5-2 order of magnitude at $T \lesssim 10^3$ K (compare the thin dash line to the thick ones in the upper panel). So that the higher initial density is the larger deviation from the isochoric case can be found. The H_2 fraction at $Z = Z_\odot$ increases about 10 times (thick grey lines in the lower panel), but the H_2 contribution to the cooling rate still remains negligible for solar metallicity. We should note that although the H_2 fraction is higher than that in the isochoric case, but this is still insufficient for CO/H_2O formation. For 10^{-3} $Z_\odot$ the dependence of ionization kinetics on initial gas density is less pronounced (thick black lines in the upper panel). It can be appreciable only at $T \lesssim 100$ K. The H_2 fraction reaches its 'universal value' and does not depend on density (thick black lines in the lower panel).

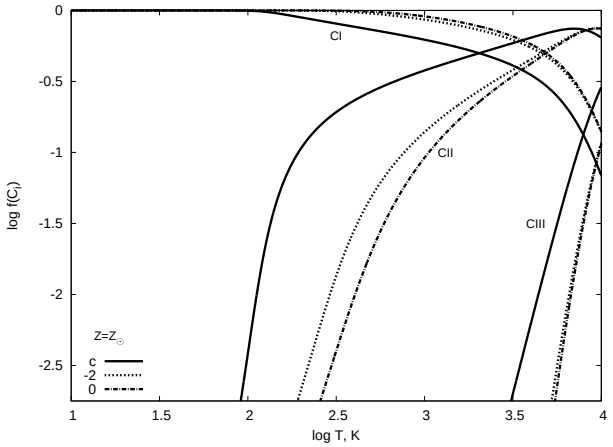

Figure 8. The CI and CII fractions in isochorically (solid line) and isobarically (dot and dash-dotted lines) cooled gas with solar metallicity. In the isochoric calculation the density of a gas is 0.1 cm^{-3} (the pressure equals $1.38 \times 10^{-13}(T/10^4\mathrm{K})$ erg cm^{-3}). In the isobaric models the initial density values are 10^{-2} cm^{-3} (the pressure is 6.9×10^{-13} erg cm^{-3}) and 1 cm^{-3} (the pressure is 6.9×10^{-11} erg cm^{-3}), depicted by dot and dash-dotted lines, respectively. The initial temperature for the isobaric calculations equals 5×10^5 K.

Figure 7 shows the contributions to the total isobaric cooling rate from major chemical elements for initial number densities $n = 1$ cm^{-3} (upper panel) and $n = 10^{-2}$ cm^{-3} (lower panel) for gas with $Z = Z_\odot$ (the contributions by N, Ne, Mg and molecules are minor in this temperature range for gas with such metallicity). We present the low-temperature part of the cooling curve, because the isobaric effects reveal in this range. One can note a strong difference between cooling rates at $T \lesssim 300$ K. The contribution by carbon, which is the main coolant for the initial density 10^{-2} cm^{-3}, is significantly suppressed for higher initial density value. One can find that at $T \lesssim 300$ K the energy losses in the fine-structure transition of CI (609 μm) dominate in the cooling, and also that the critical density (when the level populations go from non-equilibrium, $L \sim n^2$, to equilibrium, $L \sim n$) of this transition is $160(T/100)^{-0.34}$ cm^{-3} (Hollenbach & McKee 1989). During isobaric contraction from 5×10^5 K to $\lesssim 300$ K the density increases more than $\gtrsim 2.3 \times 10^3$ times. So that at $T \lesssim 300$ K the cooling of gas with initial density $n = 10^{-2}$ cm^{-3} should be more efficient (where $L \sim n^2$) than that of gas with initial density $n = 1$ cm^{-3} (where $L \sim n$).

As an example we consider the carbon ionization kinetics in detail. Figure 8 present the carbon ionization states for a gas with solar metallicity cooled isochorically (solid line) and isobarically (dot and dash-dotted lines). In the isobaric models the CI fraction is about 1 at $T \lesssim 300$ K. Then, there are no other coolants except CI in this temperature range (Figure 7), and the difference between the cooling rates (Figure 7) is explained by the equilibration of the CI level populations. Similar effect can be found for CII within $T \sim 300 - 10^4$ K, but it is less pronounced than that for CI. In general, a decrease of pressure (or initial density with fixed initial temperature) leads to that the isobaric cooling

rate tend to the isochoric one (see e.g. Figure 5). For low-metallicity gas the role of metals to cooling rate diminishes and the transition becomes less distinguishable, because the critical density for the H_2 roto-vibrational levels is higher, it is about 10^4 cm^{-3}. In the presence of UV radiation this transition can be significant in diffuse clouds in the interstellar medium (see e.g. Liszt 2011).

5 APPLICATION: SUPERNOVA EXPLOSION

In the previous sections we have considered the cooling rates of gas cooled from $T \gtrsim 5\times10^5$ K. These conditions naturally correspond to a gas behind strong shock waves originated in collisions of galaxies, virial shocks in clusters of galaxies and, more common and usual process in the interstellar gas, supernova (SN) explosions. The temperature of gas just behind SN shockwave is generally higher than 5×10^5 K, so that the cooling rates calculated in this paper are valid for physical conditions behind SN shockwave. To study the SN evolution we use the multi-dimensional parallel code ZEUS-MP (Hayes et al. 2006). We have added the cooling processes into the energy equation using the explicit four-step Runge-Kutta method.

The upper panel of Figure 1 shows that in the high-temperature regime ($T \gtrsim 10^4$ K) the cooling rate calculated in this work is close to that obtained in other studies. A significant difference of the rates can be found in the low-temperature regime ($T \lesssim 10^4$ K). Certainly, the difference between cooling rates more than 2-3 times can lead to earlier (or later) beginning of the radiative phase of a SN shell and, as a result, different scales of fragments appeared due to thermal instability. In general, gasdynamic simulations with self-consistent chemical kinetics undoubtedly trace any variation of cooling rate due to both chemical transformation and gas dynamics, but such calculations are very time-consuming, restricted in resolution (one should include multi-species advection in gas dynamics) and in applications (one should take into account valid chemical species and processes for a given physical task).

Use of tabulated cooling rates gives more flexibility in study of some physical processes. One of them is mixing metals in the interstellar/intergalactic medium (Ferrara et al. 2000; de Avillez & Mac Low 2002; Dedikov & Shchekinov 2004; Scalo & Elmegreen 2004; Vasiliev et al. 2009; Ntormousi & Burkert 2011; Vasiliev et al. 2012). Metals are produced in stellar interiors and ejected into surroundings by supernova explosions. But available data for cooling rates (Sutherland & Dopita 1993; Gnat & Sternberg 2007; Schure et al. 2009; Wiersma et al. 2009) are very constrained in metallicity and temperature, or even combined from different sources (Schure et al. 2009). Of course, one can utilize pre-computed tables assumed the equilibrium (e.g. use CLOUDY, see Wiersma et al. 2009) or choose several species for nonequilibrium calculations, whereas others are considered in equilibrium (e.g. Smith et al. 2008). But in the former we have equlibrium rates, which significantly differ from the nonequilibrium ones, whereas the latter needs a significant computational time.

Besides our cooling rates Figure 1 presents two other cooling curves at $T < 10^4$ K: Spaans & Norman (1997) and Dalgarno & McCray (1972). The former differs slightly from the rate calculated here at $T \gtrsim 10^2$ K, so we don't consider it. The latter widely used in the ISM studies (e.g., de Avillez & Mac Low 2002; Ntormousi & Burkert 2011) is valid only at $T < 10^4$ K and demonstrates significant differences from ours for $x_e \lesssim 0.1$. So that we use the cooling rates calculated in this paper in high temperature range, $T > 10^4$ K, whereas for $T < 10^4$ K we take three options for cooling rate: a) our self-consistent isochoric calculations (label 'NEQ'), b) the Dalgarno & McCray (1972) rate for the fixed electron fraction $x_e = 0.1$ (label 'NEQ+DMC72, $x_e = 0.1$') and c) the same rate, but for $x_e = 10^{-4}$ (label 'NEQ+DMC72, $x_e = 10^{-4}$'). Our choice of x_e is explained that the rate for higher value x_e is close to our rate at $T \sim 10^3-10^4$ K, whereas the lower x_e is close to the value that Smith et al. (2008) found for the interstellar gas with solar abundance (the same value can be obtained for gas ionized by cosmic rays in the local ISM, see e.g. Wolfire et al. 1995).

Here we investigate the dependence of the SN shell evolution in a homogeneous medium with solar metallicity on different cooling rates in low temperature range, $T < 10^4$ K. We have carried out the 2D gasdynamic simulations (cylindrical geometry) of a SN explosion. The numerical resolution is 1000×1000, that corresponds to the physical size of a cell 0.4 pc. The SN energy is initially injected in the central region with radial size 3.2 pc, the total energy is 10^{51} erg. To exclude the evolution of the gas in the medium before shockwave we set the temperature of this gas to 50 K and do not allow to cool it down. The differences of the SN shell evolution due to variation of the cooling rate can be found just after time $t \sim 10^{13}$ s, when initially hot shell cooled to $\sim 10^4$ K. We continued the calculations as long as $t = 10^{14}$ s, at this time various instabilities destroy SN shell, but here we are interested in the beginning of the shell evolution cooled below 10^4 K. At $t \lesssim 3\times10^{13}$ s the shell is still close to spherical shape, so that we can present radial distributions of physical quantities only.

Figure 9 present the radial distributions of density (upper) and temperature (lower) around a SN exploded in a homogeneous medium with density $n = 3\times10^{-2}$ cm^{-3} and solar metallicity for different cooling rates at $T < 10^4$ K. At $t = 1.4\times10^{13}$ s (the left row of panels in Figure 9) one can find that the radiative phase begins in the SN shell cooled with the rate calculated in this work ('NEQ') and the Dalgarno & McCray (1972) rate for the fixed electron fraction $x_e = 0.1$ ('NEQ+DMC72, $x_e = 0.1$'). In the first ('NEQ') model the thin shell is formed, the density in the shell increases in several times and the temperature is low as ~ 100 K. Whereas in the second ('NEQ+DMC72, $x_e = 0.1$') model the effects of radiative cooling begin to become apparent only: the radiative phase have just begun. The main difference between two models is the absence of temperature plateau at $T \simeq 10^4$ K in case of the self-consistent cooling rate ('NEQ'). The plateau (see radial distances $r \sim 200-250$ pc) originates from lower cooling rate in the 'NEQ+DMC72, $x_e = 0.1$' model in comparison with the rate used in the 'NEQ' model. At $t = 1.6\times10^{13}$ s the SN shell becomes radiative for the 'NEQ+DMC72, $x_e = 0.1$' model. A gas in the shell begins to cool below 10^4 K, and the plateau in the radial temperature distribution disappears gradually. In the third ('NEQ+DMC72, $x_e = 10^{-4}$') model considered here a gas in the shell starts to cool down below 10^4 K only

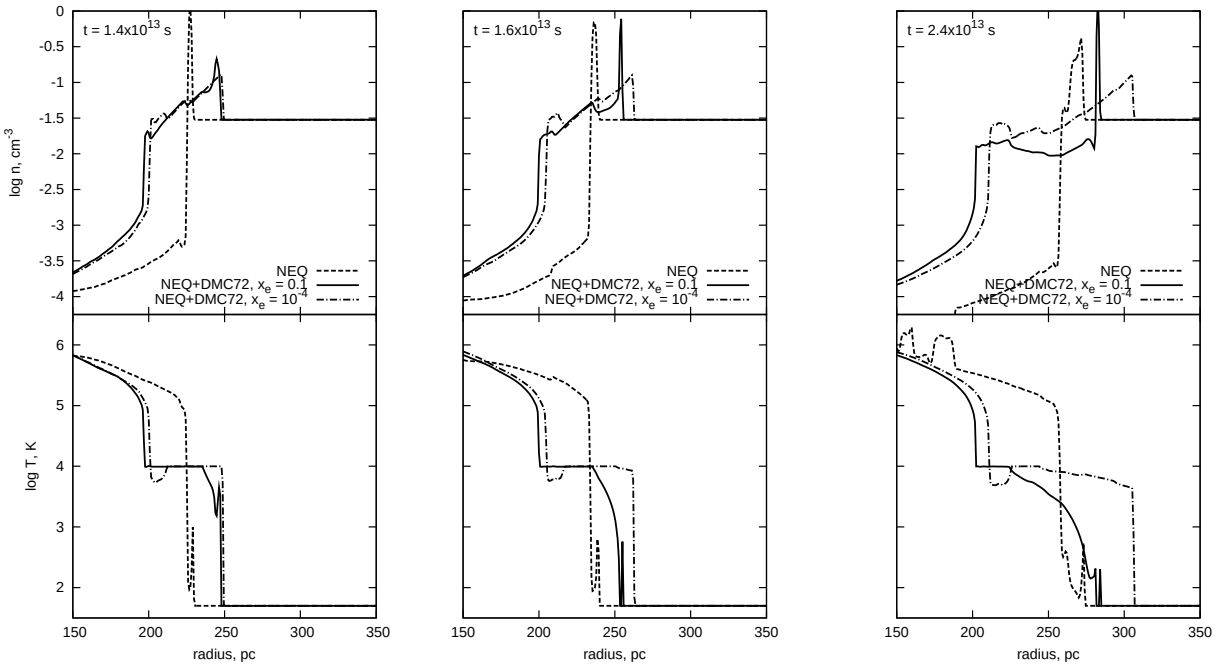

Figure 9. The radial distributions of density (upper panels), temperature (lower panels) around a SN exploded in a homogeneous medium with $n = 3 \times 10^{-2}$ cm^{-3} and solar metallicity for cooling rates in low temperature range, $T < 10^4$ K: a) the self-consistent calculations presented in this paper (solid lines), b) the Dalgarno & McCray (1972) rate for the fixed electron fraction $x_e = 0.1$ (dashed lines) and c) the same rate, but for $x_e = 10^{-4}$ (dotted lines). Left column panels shows the distributions at $t = 1.4 \times 10^{13}$ s after explosion, middle column presents the same at $t = 1.6 \times 10^{13}$ s and right column of panels shows the same at $t = 2.4 \times 10^{13}$ s. In high temperature range, $T > 10^4$ K, we use the cooling rates calculated in this work.

at $t = 2.4 \times 10^{13}$ s (right column of panels in Figure 9). This delay can be easily explained by lack of cooling at $T \sim 10^4$ K in the 'NEQ+DMC72, $x_e = 10^{-4}$' model in comparison with the other models considered in this section (Figure 1). Note that this delay can significantly affect on the SN hot bubble dynamics: the hot bubble has different sizes depending on the cooling curve assumed in calculation. This can be apparent in mixing metals, because the metals ejected by SN are initially confined in the hot bubble. Thus, we can conclude that tabulated cooling rates should be used carefully, because some gaseous structures may form due to using cooling rates cooling rates calculated for different physical conditions. As far as possible one should use cooling rates calculated self-consistently for the whole temprature range of one's interest.

6 CONCLUSIONS

In this paper we have presented self-consistent calculations of the non-equilibrium cooling rates of a dust-free collisionally controlled gas with metallicities in the range $10^{-4}\ Z_\odot \leqslant Z \leqslant 2\ Z_\odot$ cooling from high temperatures $T > 5 \times 10^5$ K down to 10 K[3]. We have found that

- molecular hydrogen dominates cooling at $10^2 \lesssim T \lesssim 10^4$ K and $Z \lesssim 10^{-3}\ Z_\odot$, its contribution around $T \sim (4-5) \times 10^3$ K stimulates thermal instability at $Z \lesssim 10^{-2}\ Z_\odot$;
- the ionization fraction remains rather high at $T \lesssim 10^4$ K: it reaches up to ~ 0.01 at $T \simeq 10^3$ K and $Z \lesssim 0.1\ Z_\odot$, and becomes higher for higher Z;
- despite high ionization fraction the abundance of molecular hydrogen decreases with metallicity;
- at $T \lesssim 10^4$ K isobaric cooling rates are lower than isochoric ones;
- in isobaric processes the ionization fraction decreases considerably and molecular hydrogen grows more efficient compare to isochoric ones.

We have compared our self-consistent cooling functions with those published in previous works and found considerable differences. In particular, we found that the two approaches for the cooling processes result in a fairly distinct dynamics of supernova remnants.

[3] The isochoric cooling rates presented in Figure 2b are available in electronic form at http://ism.rsu.ru/cool/coolfun.html.

7 ACKNOWLEDGEMENTS

The author thanks the anonymous referee for valuable comments. The author is grateful to Yuri Shchekinov for help and many useful discussions, Mikhail Eremin and Eduard Vorobyov for stimulating discussions, Ilya Khrykin for his assistance. Gary Ferland and CLOUDY community are acknowledged for creating of the excellent tool for study photoionized plasma. This work is supported by the RFBR through the grants 12-02-00365, 12-02-00917, 12-02-90800, and partially 12-02-92704, 11-02-01332, 11-02-97124, and by

the Russian federal task program Research and operations on priority directions of development of the science and technology complex of Russia for 2009-2013 (state contract 14.A18.21.1304). The author is grateful for support from the "Dynasty" foundation.

REFERENCES

Abel T., Anninos P., Zhang Yu., Norman M.L., 1997, NewA, 2, 181
Asplund, M., Grevesse, N., & Sauval, A. J. 2005, in ASP Conf. Ser. 336, Cosmic Abundances as Records of Stellar Evolution and Nucleosynthesis, ed. T. G. Barnes III & F. N. Bash (San Francisco: ASP), 25
Benjamin R. A., Benson B. A. & Cox D. P., 2001, ApJ, 554, L225
Böhringer H. & Hensler G., 1989, A&A, 215, 147
Brown P. N., Byrne G. D., & Hindmarsh A. C., 1989, SIAM J. Sci. Stat. Comput., 10, 1038
Bryans P., Badnell N. R., Gorczyca T. W., Laming J. M., Mitthumsiri W., Savin D. W., 2006, ApJS, 167, 343
Burkert A. & Lin D.N.C., 2000, ApJ, 537, 270
Cazaux S. & Tielens A.G.G.M., 2004, ApJ, 604, 222
Chevalier R.A. & Imamura J.N., 1982, ApJ, 261, 543
Cox D. P., & Tucker W. H. 1969, ApJ, 157, 1157
Dalgarno A. & McCray R. A., 1972, ARA&A, 10, 375
de Avillez M. A. & Breitschwerdt D., 2010, ASP Conf. Ser., 438, 313
de Avillez M. A. & Mac Low M.-M., 2002, ApJ, 581, 1047
Dedikov S.Yu., Shchekinov Yu.A., 2004, Astr. Rep., 48, 9
Dopita M. A. & Sutherland R. S., 1996, ApJS, 102, 161
Draine B. T. & Salpeter E. E., 1979, ApJ, 231, 77
Drake J. J. & Testa P., 2005, Nature, 436, 525
Edgar R. J. & Chevalier R. A., 1986, ApJ, 310, L27
Ferland G. J., Korista K. T., Verner D. A., Ferguson J. W., Kingdon J. B. & Verner E. M. 1998, PASP, 110, 761
Ferrara A., Pettini M., Shchekinov Yu.A., 2000, MNRAS, 319, 539
Flower D., 2000, MNRAS, 318, 875
Gaetz T. J. & Salpeter E. E., 1983, ApJS, 52, 155
Galli D. & Palla F., 1998, A&A, 335, 403
Glover S.C.O., 2003, ApJ, 584, 331
Glover S.C.O. & Jappsen A.-K., 2007, ApJ, 666, 1
Gnat O. & Sternberg A., 2007, ApJS, 168, 213
Hayes J.C., Norman M.L., Fiedler R.A., Bordner J.O., Li P.S., Clark, S.E., ud-Doula A., Mac Low M.-M., 2006, ApJS, 165, 188
Hollenbach D. & McKee C. F., 1979, ApJS, 41, 555
Hollenbach D. & McKee C. F., 1989, ApJ, 342, 306
House L. L., 1964, ApJS, 8, 307
Izotov Yu.I. & Thuan T.X., 1998, ApJ, 500, 188
Kafatos M., 1973, ApJ, 182, 433
Landi E. & Landini M., 1999, A&A, 347, 401
Lipovka A., Núñez-López R., Avila-Reese V., 2005, MNRAS, 361, 850
Liszt H.S., 2011, A& A, 527, 45
Mac Low M.-M. & Shull J.M., 1986, ApJ, 302, 585
Ntormousi E. & Burkert A., 2011, ApJ submitted, arXiv1111.1859
Oh S.P. & Haiman Z., 2002, ApJ, 569, 558
Olive K., 2010, arXiv:1005.3955
Omukai K., Tsuribe T., Schneider R., Ferrara A., 2005, ApJ, 626, 627
Raymond J. C., Cox D. P. & Smith B. W. 1976, ApJ, 204, 290
Scalo J. & Elmegreen B.G., 2004, ARA&A, 42, 275
Schmutzler T. & Tscharnuter W. M., 1993, A&A, 273, 318
Schure K.M., Kosenko D., Kaastra J.S., Keppens R., Vink J., 2009, A&A 508, 751
Shapiro P.R. & Kang H., 1987, ApJ, 318, 32
Shapiro P. R. & Moore R. T., 1976, ApJ, 207, 460
Shchekinov Yu.A., 1978, SvA, 22, 182
Shull J. M. & van Steenberg M., 1982, ApJS, 48, 95
Smith B., Sigurdsson S., Abel T., 2008, MNRAS, 385, 143
Spaans M. & Norman C., 1997, ApJ, 483, 87
Stancil P.C., Lepp S., Dalgarno A., 1998, ApJ, 509, 1
Sutherland R. S. & Dopita M. A., 1993, ApJS, 88, 253
Vasiliev E. O., 2011, MNRAS, 414, 3145
Vasiliev E. O., 2012, MNRAS, 419, 3641
Vasiliev E.O., Dedikov S.Yu., Shchekinov Yu.A., 2009, Astr. Bull., 64, 317
Vasiliev E.O., Vorobyov E.I., Matvienko E.E., Razoumov A.O., Shchekinov Yu.A., 2012, Astr. Repts, 56, 895
Verner D. A., Ferland G. J., Korista K. T. & Yakovlev D.G., 1996, ApJ, 465, 487
Wiersma R., Schaye J., Smith B.D., 2009, MNRAS, 393, 99
Wolfire M.G., Hollenbach D., McKee C.F., Tielens A.G.G.M., Bakes E.L.O., 1995, ApJ, 443, 152

APPENDIX A: MOLECULAR HYDROGEN AND DEUTERIUM CHEMISTRY

In this section we present the minimal model of chemical kinetics for molecular hydrogen and deuterium in the low temperature range, $T < 2\times10^4$K. We include collisional gas-phase reactions only. The reactions are listed in Table A1. This model is based on the well-tested minimum models for molecular hydrogen and deuterium chemistry for both primordial (Abel et al. 1997; Galli & Palla 1998) and metal-enriched (Omukai et al. 2005; Glover & Jappsen 2007) gas. We don't list here the helium chemistry, because it consists of collisional ionization and recombination only, these processes are inevitable part of our model and the references to reactions can be found in (Vasiliev 2011). Other helium species, like HeH^+, cannot change thermal evolution of a gas significantly, so that we do not include its in the model.

Table A1. Chemical reaction rates

reaction	Reference
H_2 chemisrty	
$H + e^- \rightarrow H^- + h\nu$	Galli & Palla (1998)
$H^- + h\nu \rightarrow H + e^-$	–
$H^- + H \rightarrow H_2 + e^-$	–
$H^- + H^+ \rightarrow H_2^+ + e^-$	–
$H^- + H^+ \rightarrow 2H$	–
$H^+ + H \rightarrow H_2^+ + h\nu$	–
$H_2^+ + H \rightarrow H_2 + H^+$	–
$H_2^+ + e^- \rightarrow 2H$	–
$H_2 + H^+ \rightarrow H_2^+ + H$	–
$H_2 + e^- \rightarrow 2H + e^-$	–
$H_2 + H \rightarrow 3H$	Mac Low & Shull (1986)
$H^+ + e^- \rightarrow H + h\nu$	Verner et al. (1996)
$H + e^- \rightarrow H^+ + 2e^-$	Abel et al. (1997)
$H^- + e^- \rightarrow H + 2e^-$	–
$H^- + H \rightarrow 2H + e^-$	Shapiro & Kang (1987)
D chemistry	
$D^+ + e^- \rightarrow D + h\nu$	Galli & Palla (1998)
$D + h\nu \rightarrow D^+ + e^-$	–
$D + H^+ \rightarrow D^+ + H$	–
$D^+ + H \rightarrow D + H^+$	–
$D + H_2 \rightarrow H + HD$	–
$D^+ + H_2 \rightarrow HD + H^+$	–
$HD + H \rightarrow H_2 + D$	–
$H^+ + HD \rightarrow H_2 + D^+$	–
$D + e^- \rightarrow D^- + h\nu$	–
$D^+ + D^- \rightarrow 2D$	–
$H^+ + D^- \rightarrow D + H$	–
$H^- + D \rightarrow H + D^-$	–
$D^- + H \rightarrow D + H^-$	–
$D^- + H \rightarrow HD + e^-$	–